Supplementary Information

S1 Preparation of the perovskite thin film and gas sensor devices

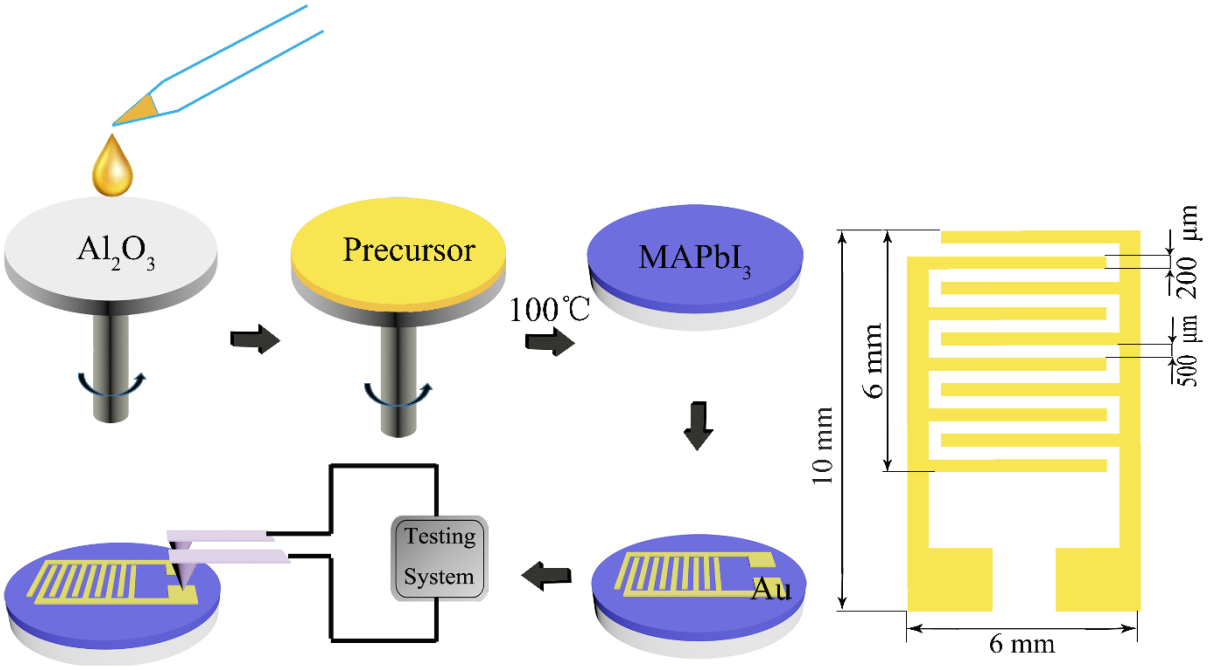

Fig. S1 Schematic illustration of the process of fabricating $MAPbI_3$ thin film and gas sensor device.

S2 Experimental setup used in characterizing the sensing performance of gas sensors

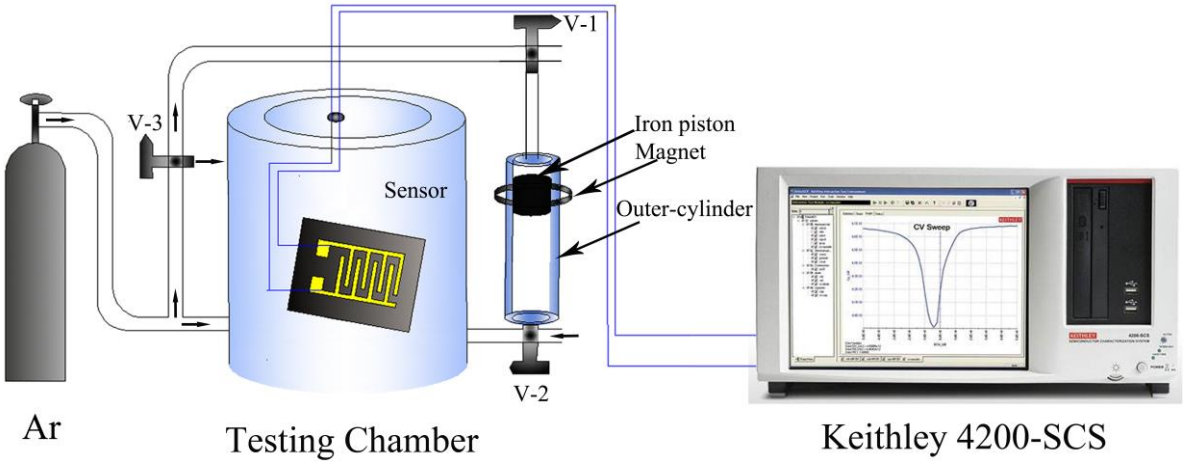

Fig. S2 Facility used for examining gas-sensing characteristics of gas sensors.

S3 Operation process of gas-sensing characterization in atmospheric pressure and high-pressure argon gas

Atmospheric pressure gas-sensing performance of the $MAPbI_3$ sensors was examined using a specially designed chamber with a capacity of 180 ml (Fig. S3a), which was electrically connected to the Keithley 4200-SCS semiconductor parameters analyzer. Fig. S3b shows the statuses of valve-1, valve-2 and valve-3 during the characterization process. Before the gas-sensing characterization, the air in the chamber was completely expelled with high purity argon gas. The entire measuring procedure went through four stages. In the first stage, valve-1 was totally switched off, and appropriate volume of target gas was injected to the outer-cylinder through port 3 of valve-2 (port 1 was connected to the outer-cylinder). In the second stage, the statuses of valve-1 and valve-3 remain unchanged, while valve-2 was totally closed, and the target gas was stored in the outer-cylinder. In the third stage, we switched on the valve-2 (target gas cylinder was connected to testing chamber) and valve-1 (testing chamber was connected to target gas cylinder). The target gas stored in the outer-cylinder was injected into the testing chamber by driving the piston downwards. At the same time, the variation in the resistance of $MAPbI_3$ film sensor was recorded by the Keithley 4200-SCS semiconductor parameter analyzer. In the fourth stage, argon gas was introduced into the testing chamber through port 2 of valve-3 to a certain pressure, and valve-3 was fully switched on to release the high-pressure gas from the chamber, carrying away the target gas. Thus the resistance of $MAPbI_3$ film sensor recovered to its original value and the characterization process was finished.

For examining the high-pressure gas-sensing performance of the $MAPbI_3$ sensors, the overall procedure includes all the above-mentioned four stages. The operation process in the first stage was the same with that mentioned above, while different operation processes were conducted from the second stage. Namely, the statuses of valve-1 and valve-3 remain unchanged while valve-2 was closed in the second stage, and the target gas was stored in the outer-cylinder. Afterwards, high-pressure argon gas was introduced into the testing chamber through port 2 of valve-3 to a designated pressure. In the third stage, port 2 of valve-1 was connected to its port 1, and port 1 of valve-2 was connected to its port 2, thus the target gas stored in the outer-cylinder was injected into the testing chamber via the downwards movement of the piston. The variation in the resistance of $MAPbI_3$ film sensor was simultaneously recorded by the Keithley 4200-SCS semiconductor parameter analyzer. In the fourth stage, valve-3 was fully switched on to release the high-pressure gas from the testing chamber, and the target gas was carried away, thus the resistance of $MAPbI_3$ film sensor recovered to its original value.

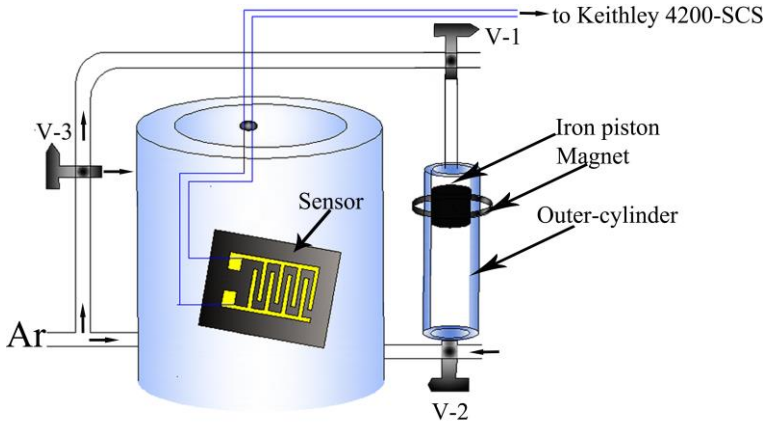

(a)

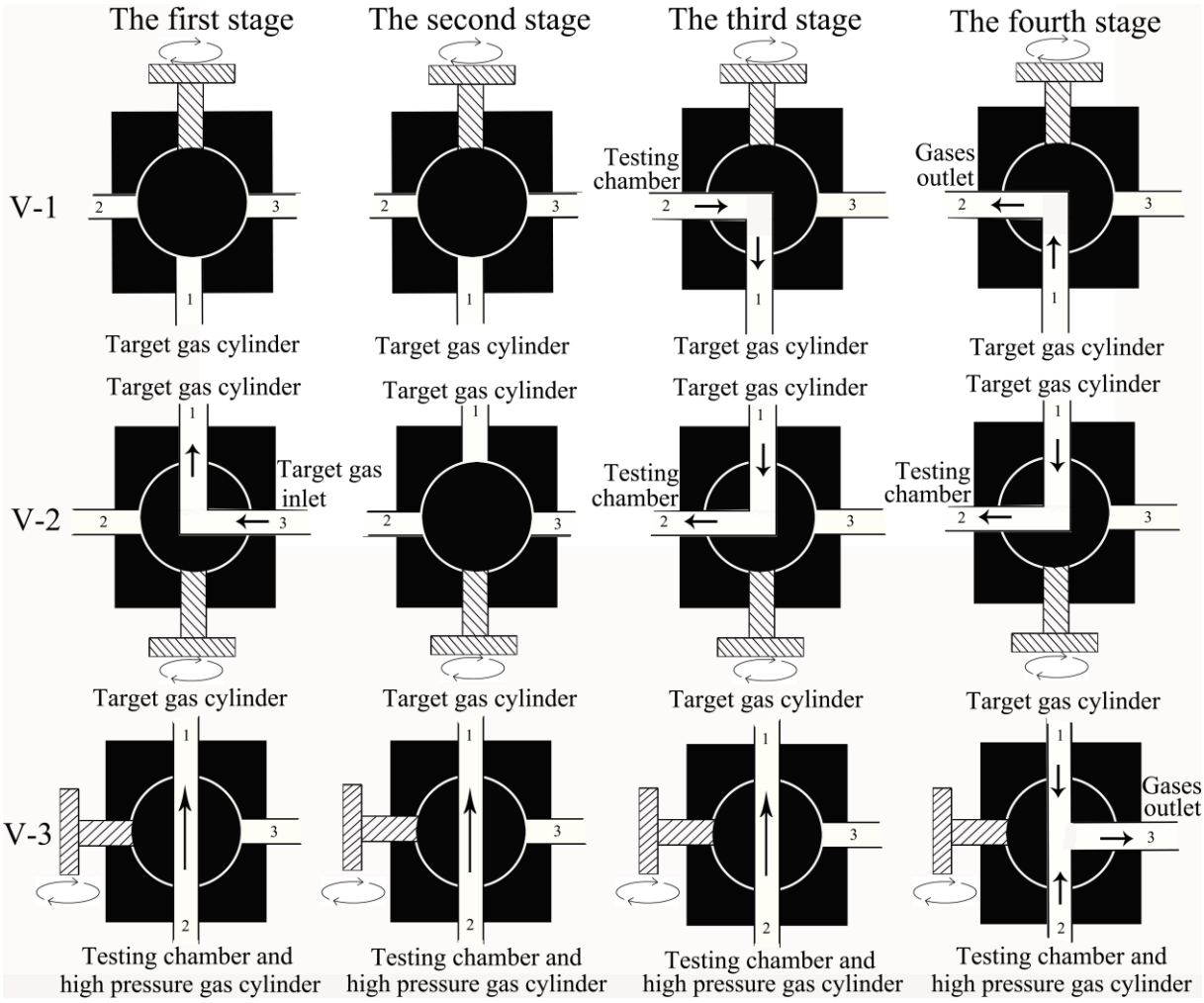

(b)

Fig. S3 (a) Structure of the facility utilized in gas-sensing characterization under high-pressure argon gas. (b) The working states of valve-1, valve-2 and valve-3 during the measuring process.

S4 Cross-sectional morphology of $MAPbI_3$ film

The image shown in Fig. S4 clearly indicates that the $MAPbI_3$ film was composed of loosely stacked nanocrystals, with a large amount of pores existing in it. The thickness of the film was about 1.5~2.0 μm. Besides, the surface of the $MAPbI_3$ film was quite rough, which benefits the improvement of gas-sensing performance to a rather large extent.

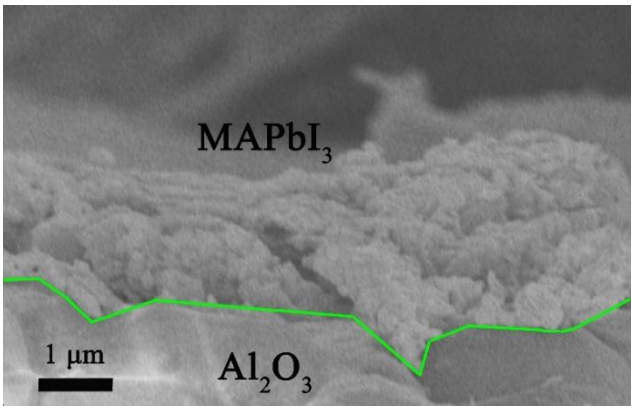

Fig. S4 Cross-sectional SEM image of the $MAPbI_3$ film. The green line indicates the interface of $MAPbI_3$ and Al_2O_3 substrate.

S5 TEM images of the $MAPbI_3$ nanoplates

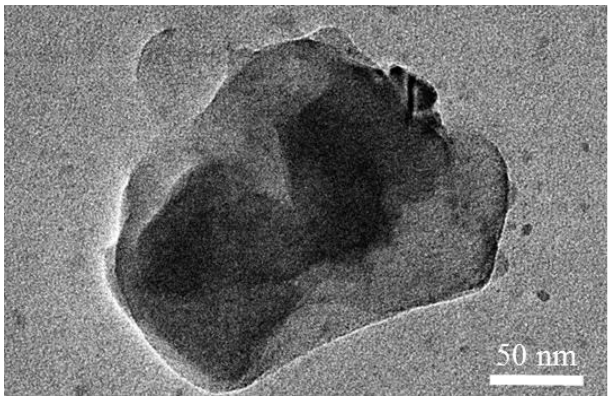

Fig. S5 TEM image of $MAPbI_3$ nanoplates.

S6 Dynamic response of $MAPbI_3$ sensor under different bias voltages

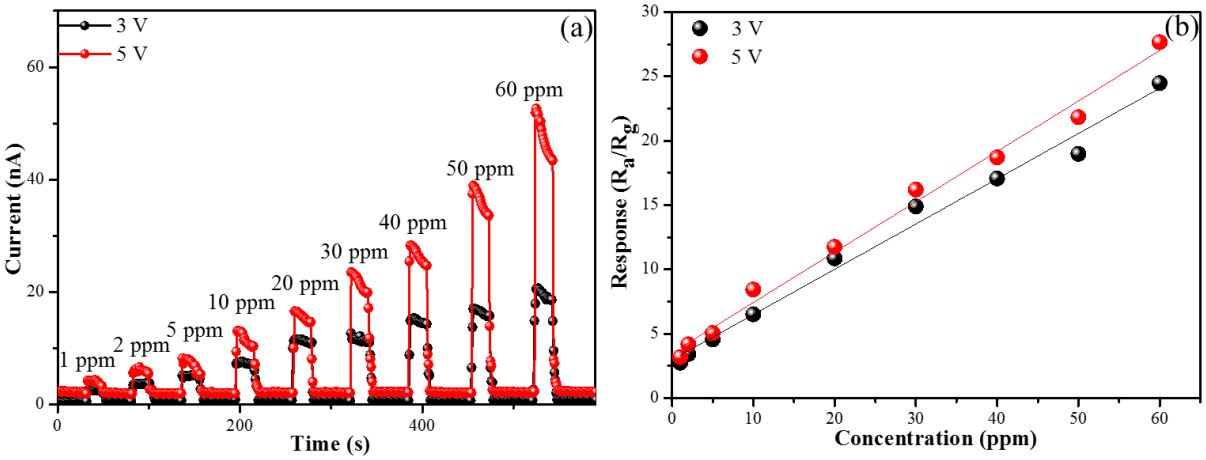

Fig. S6 (a) Dynamic response curves of $MAPbI_3$ film sensor to NO_2 (1~60 ppm) gas and (b) Response of $MAPbI_3$ film sensor vs concentration of NO_2 under different bias voltages.

Fig. S6 clearly shows that the current and response through the gas sensor strikingly increase when the bias voltage improved from 3 V to 5 V.

S7 Reproducibility of $MAPbI_3$ sensor

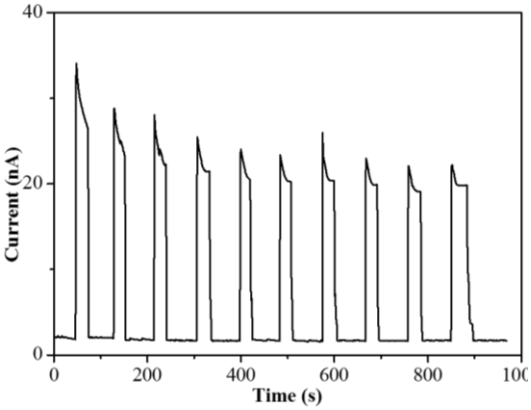

Fig. S7 Reproducibility of $MAPbI_3$ sensor in ambient circumstance with relative humidity of 35%.

In order to examine the reproducibility of the $MAPbI_3$ film sensor in ambient circumstance, we repeatedly introduced NO_2 gas (30 ppm) into the testing chamber and then evacuated it for many times. The corresponding results of the first 10 circles are presented in Fig. S7. The current of the sensor decays slightly within the first four circles. After that, it remains almost constant, revealing quite good reproducibility of the $MAPbI_3$ film sensor when it is exposed to moisture.

S8 Dynamic response of $MAPbI_3$ film sensor to different target gases under ambient pressure

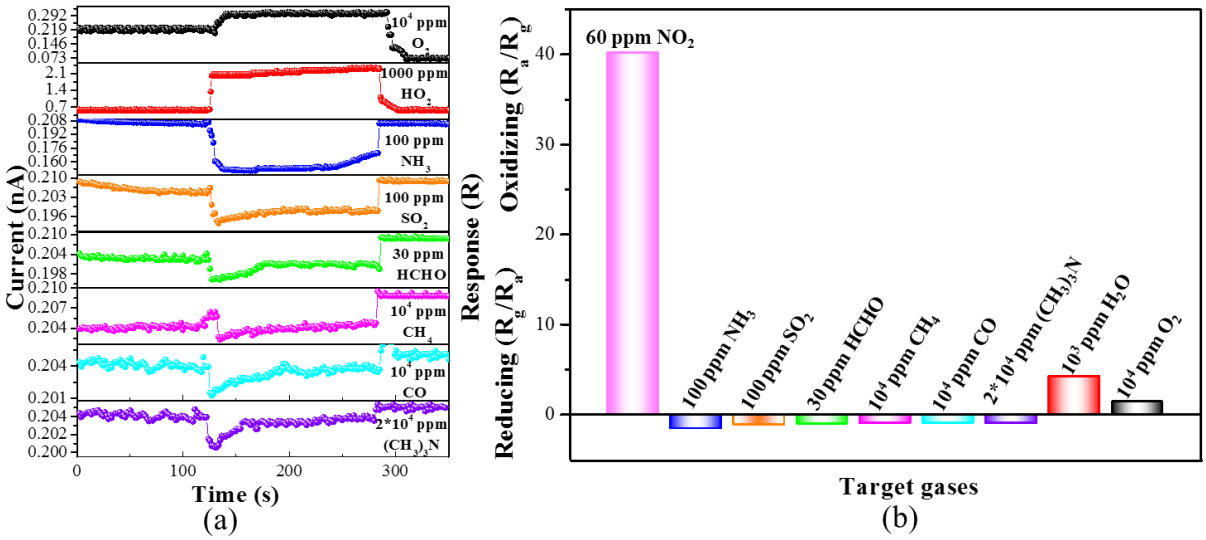

Fig. S8 Dynamic response and recovery curves and response of $MAPbI_3$ film sensor to different target gases at ambient pressure.

The $MAPbI_3$ film sensor exhibited excellent selectivity towards NO_2 gas when other reference gases coexisted. By comparing Fig. 2, 3 and S8, two distinct differences could be clearly observed. Firstly, the response way of $MAPbI_3$ film sensor towards NO_2 gas was opposite to that towards other reference gases except for H_2O and O_2. Namely, the current of this sensor predominately increased when the NO_2 was introduced into the testing chamber. Secondly, the response of $MAPbI_3$ film sensor to NO_2 was much higher than that to all the other reference gases. These characteristics endowed $MAPbI_3$ film sensor rather high reliability when being used as the NO_2 gas sensor.

S9 Calculation of NO_2 adsorption energy on the perovskite surface under different pressures

The adsorption energy of the NO_2 on the perovskite surface under different pressures were calculated by using the FORCITE package in the Materials Studio. The COMPASS (Condensed-phase Optimized Molecular Potentials for Atomistic Simulation Studies) refer force-field was used to describe the interaction between NO_2 and the surface atoms of perovskite. As for the situation in which NO_2 interacted with perovskite, the (110) surface was created by periodical replication of an elementary cell in both x and y directions, where periodical condition was applied. The pressures for the simulation process were set to 0.1 MPa (atmosphere pressure), 4 MPa and 8 MPa. The thickness of the vacuum slab was set to be 30 Å in order to avoid unnecessary interactions between adjacent layers. NPT ensemble with simulation time of 100 ps was used to run the test, and the step was maintained to 1 fs. The initial structure for the molecular dynamics simulation was presented as follows:

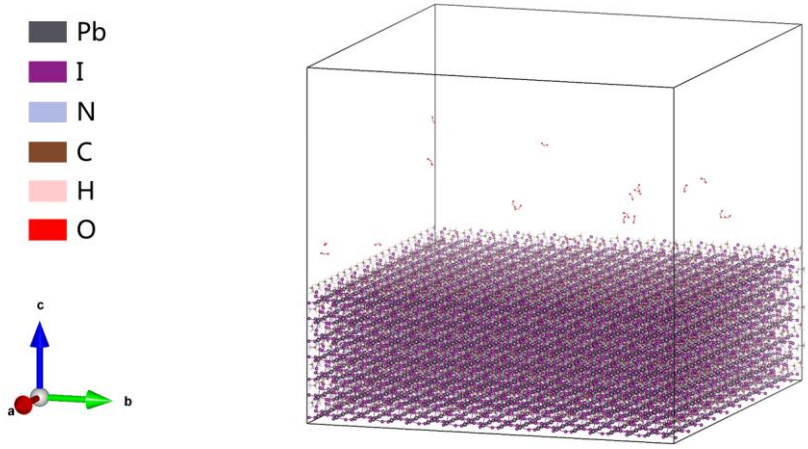

The calculated results was presented in Figure S9. The adsorption energy was defined as:

$$E_{ad} = E_{tot} - (E_{sur} + E_{NO_2})$$

in which E_{ad} is the adsorption energy between the perovskite surface and NO_2 molecules, E_{tot} is the total energy of the simulation system, including the pervoskite surface and NO_2 molecules, E_{sur} is the surface energy of the perovskite (110) facet, E_{NO_2} is the energy of the NO_2 molecules in the simulation system.

The results of the molecular dynamics simulation indicated the preferential adsorption behavior of NO_2 molecules on the perovskite surface when the system was exposed under high pressure, which was consistent with the conclusion we gave in the manuscript.

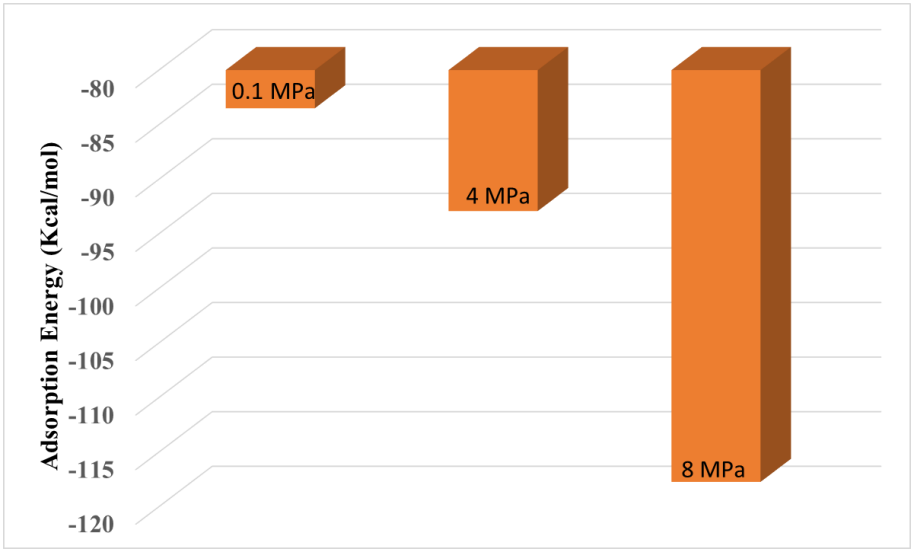

Fig. S9 The calculated adsorption energy of NO_2 molecules on the perovskite surface under different pressures.

S10 The calculation error of NO_2 film gas sensor in high pressure argon

Pressure (p, MPa)	The molar number of argon (n, mol)	The molar number of NO_2 (n_t, mol)	The volume of target gas (1% NO_2 +99% Ar) (V, ml)	The concentration of NO_2 (c_t, ppm)
0.1	n_0	n_{t0}	0.09	5
1	$10n_0$	$10n_{t0}$	0.9	5
2	$20n_0$	$20n_{t0}$	1.8	5
3	$30n_0$	$30n_{t0}$	2.7	5
4	$40n_0$	$40n_{t0}$	3.6	5
5	$50n_0$	$50n_{t0}$	4.5	5
6	$60n_0$	$60n_{t0}$	5.4	5
7	$70n_0$	$70n_{t0}$	6.3	5
8	$80n_0$	$80n_{t0}$	7.2	5

Here n_0 is the molar number of argon gas at atmospheric pressure. p_0 is the atmospheric pressure. n_{t0} is the molar number of NO_2 under atmospheric pressure. V is the volume of NO_2 injected into the testing chamber. c_t is the molecular number concentration of NO_2 and it remained at 5 ppm at all the pressures. V_0 is the volume of testing chamber, δ is the calculation error of NO_2 film gas sensor under high pressure argon. We treat Ar and NO_2 gases as ideal gases, which meet the ideal gas equation ($pV = nRT$).

$$n_0 = \frac{p_0 V_0}{RT} = \frac{1.01325*10^5*180*10^{-6}}{298.15*8.314} = 0.007358\ mol \quad (1)$$

$$n_{t0} = \frac{p_0 V}{RT}*1\% = \frac{1.01325*10^5*0.09*10^{-6}}{298.15*8.314}*1\% = 3.67887\times10^{-8}\ mol \quad (2)$$

$$\delta = \frac{c_t^{calc} - c_t^{real}}{c_t^{real}} = \frac{\frac{n_t}{n} - \frac{n_t}{n+n_t}}{\frac{n_t}{n+n_t}} = \frac{n_t}{n} \quad (3)$$

p_0 = 101325 *Pa*, $V_0 = 1.8*10^{-4}\ m^3$, R = 8.314 $Pa{\cdot}m^3/mol{\cdot}K$, T=298.15 *K*.

c_t^{calc} is the molecule number concentration of target gases ignoring the molar number of NO_2.

c_t^{real} is the molecule number concentration of target gases considering the molar number of NO_2.

According to the formula (1), (2) and (3), δ is a constant under different pressures.

$$\delta = \frac{n_t}{n} = \frac{n_{t0}}{n_0} = 0.005‰$$

S11 The sensitivity of $MAPbI_3$ film sensor to different target gases in high-pressure argon

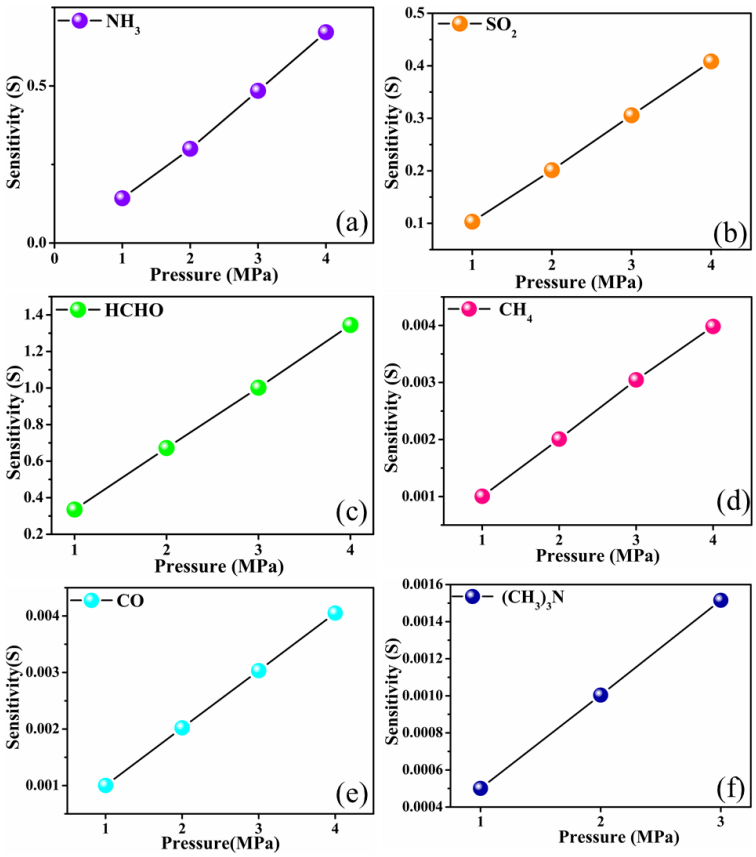

Fig. S11 The sensitivity of $MAPbI_3$ film sensor to reference gases under high pressure.

Fig. S11 clearly indicated that the sensitivities of $MAPbI_3$ film sensor to all the reference gases were rather lower than that of NO_2, revealing that this sensor still possesses excellent selectivity even under high-pressure.